Bioorganic Chemistry 90 (2019) 103028

Contents lists available at ScienceDirect

Bioorganic Chemistry

journal homepage: www.elsevier.com/locate/bioorg

Discovery of novel indole-based aroylhydrazones as anticonvulsants: Pharmacophore-based design

Violina T. Angelova[a,*], Miroslav Rangelov[b], Nadezhda Todorova[c], Miroslav Dangalov[b], Pavlina Andreeva-Gateva[d], Magdalena Kondeva-Burdina[a], Valentin Karabeliov[a], Boris Shivachev[e], Jana Tchekalarova[f,*]

[a] Faculty of Pharmacy, Medical University-Sofia (MU-Sofia), Bulgaria
[b] Institute of Organic Chemistry with Centre of Phytochemistry, Bulgarian Academy of Sciences (BAS), Sofia, Bulgaria
[c] Institute of Biodiversity and Ecosystem Research, BAS, Sofia, Bulgaria
[d] Department of Pharmacology and Toxicology, Medical University of Sofia, Bulgaria
[e] Institute of Mineralogy and Crystallography, BAS, Sofia, Bulgaria
[f] Institute of Neurobiology, BAS, 1113 Sofia, Bulgaria

ARTICLE INFO

Keywords:
Melatonin derivatives
Anticonvulsants
Neurotoxicity
Hepatotoxicity
Rodents

ABSTRACT

A number of novel melatonin derivatives, containing aroylhydrazone moieties, were synthesized and explored *in vivo* for anticonvulsant activity, neurotoxicity in ICR mice as well as *in-vitro* for cytoxicity and oxidative stress in rats. The structures and configurations were confirmed by NMR, FTIR, HRMS and crystal X-ray diffraction method. For selection of potent structures for synthesis a pharmacophore model was used. Two compounds **3e**, with a 2-furyl moiety fragment and **3f** with 2-thienyl fragment, showed a potency in maximal electroshock (MES) test (ED_{50} = 50.98 mg kg^{-1}, PI > 5.88 and ED_{50} = 108.7 mg kg^{-1}; PI > 2.76), respectively, higher than melatonin (ED_{50} = 160.3 mg kg^{-1}, PI > 1.87). The compounds **3c**, **3e, 3f** and **3i** suppressed psychomotor seizures in the 6 Hz test and **3c** was the most potent with higher ED_{50} = 13.98 mg kg^{-1} and PI of > 21.46 compared to that of melatonin (ED_{50} = 49.76 mg kg^{-1} and PI of > 6.03) in mice. None of the compounds displayed neurotoxicity in the rota-rod test. The novel melatonin derivatives exerted weak cytotoxic effects while **3f** showed the lowest hepatoxic effects comparable to that of the positive control melatonin in rats. The high affinities to the elucidated pharmacophore model of the novel melatonin compounds derived from the inclusion of aroylhydrazone moiety in the indole scaffold yielded suitable candidates with anticonvulsant activity in the MES and 6 Hz test of psychomotor seizures.

1. Introduction

Melatonin (MT) (*N*-acethyl-5-methoxytryptamine), secreted from the pineal gland during the dark period, is an important signaling hormone responsible for the fine-tuning regulation of circadian rhythms through activation of the G protein-coupled membrane melatonin MT_1 and MT_2 receptors, respectively, in mammals [1]. Endogenous hormone plays a crucial role in the regulation of sleep rhythms and can exert strong antioxidant, anti-inflammatory effects as well as neuroprotection [2]. The anticonvulsant activity of melatonin is verified in a number of seizure tests in naive rodents [3] and in models of epilepsy [4]. The use of melatonin as a drug is limited by its short half-life (15–20 min), poor oral bioavailability and the lack of selectivity at its target sites, MT1 and MT2 receptor subtype [5]. In patients with epilepsy, it was used as add-on therapy in a few clinical trials [6]. With few exceptions, the majority of clinical findings revealed that melatonin supplementation is beneficial in children with epilepsy because of its advantage, compared to classical drugs used for epilepsy, to improve sleep quality, attenuate cellular oxidative stress, lack of toxicity and ability easily to cross the blood-brain barrier (BBB) [7]. A synthetic and selective melatonin receptor agonist ramelteon was reported also to possess anticonvulsant properties [5]. The discovery of selective ligands targeting the MT1 or the MT2 melatonin receptors may promote the development of novel and more efficacious therapeutic agents with anticonvulsant action.

MT receptors are part of the G-protein coupled receptors (GPCRs) family, known as versatile signaling molecules, participating as signal transducers in different signaling pathways. Its physiological regulation

* Corresponding authors.
E-mail addresses: violina_stoyanova@abv.bg (V.T. Angelova), janetchekalarova@gmail.com (J. Tchekalarova).

https://doi.org/10.1016/j.bioorg.2019.103028
Received 11 January 2019; Received in revised form 29 May 2019; Accepted 31 May 2019
Available online 08 June 2019
0045-2068/

depends on complex mechanisms, such as the difference in affinity between the active and inactive states of the receptor and its connectivity to the G-proteins [8]. The MT1 receptor is difficult to be crystallized and its crystal structure is currently not available. Another hurdle is connected to the sequence identity, that is lower than 30% between MT receptors and the closest crystallized GPCRs. Although several 3D models exist, they are difficult to be made and key features are missing [9]. Even the possible models the complexity of the molecular mechanism of receptor interactions still make important features of its functioning not visible, as being dependent on dynamic properties [10].

As there is no available correct and adequate model of MT receptors, this lack seriously compromises the docking procedures as a methodology for the search of ligands with good binding abilities. Therefore we decided to use another approach. Since there are known specific ligands for MT receptors and based on their ability to connect to them, in their conformational spaces should exist conformations sharing similar spatial and electronic properties. These characteristics should also be shared with the new drug candidates. In this study, we used pharmacophore models as a relevant methodology to extract such spatial data from known existing ligands and to build model, in which new possible candidates can be checked.

Based on the finding that the MT receptors are potential novel targets for anticonvulsant drug development, we elucidated the pharmacophore model of MT1 receptor and this model was used for refining potential drug candidates from spatial data of available drug structures targeting the MT1 receptor. The novel indole derivatives were synthesized and explored *in vivo* for anticonvulsant activity and neurotoxicity in mice as well as *in vitro* for hepatotoxicity in rats.

2. Results and discussion

2.1. Chemistry

The synthesis of the novel series of indole C-3 substituted aroylhydrazones **3a-i** were prepared by condensation of the hydrazides **2a-i** with corresponding 5-substituted indole-3-carbaldehydes **1** as outlined in Scheme 1 and the structures were identified by their melting points, FTIR, ^{1}H NMR, ^{13}C NMR, and HRMS spectral data.

Stereochemistry was unambiguously confirmed with the help of cross-peak intensities observed in 2D NOESY spectrum. Although the four isomers were considered [11] for the aroyl hydrazones with indole scaffold, *E/Z* isomerization was generally not observed and the Z geometric isomers were absent. The ^{1}H NMR spectra of compound **3h** taken in DMSO-d_6 at 20 °C shows 1:1 mixture of conformers (*syn/anti* amide conformers). According to the confirmed NOE's between the methylidene proton and the NH proton and between the CONH proton and H-2/H-6 protons in aryl hydrazones, the most stable were *E* isomers around C=N double bond and the *synperiplanar* conformer around the amide O=C−N−N bond. Therefore, we concluded that a single *E* geometrical isomer and the observed duplication pattern of novel hydrazone derivatives to be due to the presence of *syn/anti* amide conformers in DMSO-d_6. Additionally, for structure elucidation purposes the NMR spectra of compound **3h** were measured at 373 K to achieve fast exchange. After cooling down to 293 K the ^{1}H NMR spectrum remained unchanged.

2.2. Single crystal X-ray diffraction

X-ray quality crystals of the solid hydrazones **3c** and **3f** were obtained as described in the experimental section. Compounds **3c** and **3f** crystalize in the monoclinic $P2_1/n$ and orthorhombic $P2_12_12_1$ space groups with one molecule in the asymmetric unit Fig. 1. and four molecules in the unit cell (Z = 4). One should note the structure of **3c** is pseudo orthorhombic with β close to 90° but attempts to solve the structure were unsuccessful. In **3f** the thiophene ring is disordered over two positions (72.3 and 27.7%) trough the rotation along C13−C14 bond. The bonds lengths, angles and torsion angles are comparable with those of other similar structures in the Cambridge Structural Database [12]. In both molecules the indole ring is nearly planar with *rmsd* of 0.004 Å. The N′-methyleneacetohydrazide fragment is almost coplanar with the indole ring (the angle between the mean planes of the indole and *N*′-methyleneacetohydrazide in **3c** and **3f** is 1.9 and 9.5°). The overlay of the molecules of **3c** and **3f** by their identical indole and *N*′-methyleneacetohydrazide fragments (atoms C1 to C13/O13, Fig. S1) shows that the thiophene and chlorobenzene fragments are similarly oriented, though the chlorobenzene moiety present in **3c** is rotated (along C13−C14 bond) to allow the formation of a CH_3…π weak intramolecular interaction (the angle between the mean planes of the indole/thiophen and indole/chlorobenzene rings is 18.7 and 65.2° respectively). The three-dimensional packing of the molecules in the crystals structures of **3c** and **3f** is stabilized through typical N12-H12…O13 hydrogen bonding interactions (Fig. S2).

2.3. Molecular modeling. Pharmacophore methodology

A pharmacophore is a set of three-dimensional molecular features that are necessary for molecular recognition of a ligand by a macromolecule. As it is defined in IUPAC pharmacophore is "an ensemble of steric and electronic features that is necessary to ensure the optimal supramolecular interactions with a specific biological target and to trigger (or block) its biological response". A pharmacophore query is a 3D arrangement of molecular features. In the absence of receptor information, it is hoped that feature geometries, common to many of the active structures would contain information, related to the important interactions between the bound conformations of the ligand and the receptor.

For the generation of pharmacophore model, we used a set of described in literature [8,9] structures that have proven activity against MT1 receptor (Fig. S3).

All molecules in the pharmacophore generation set can exist in different conformations and we have no data for the preferred ones in the active site of the MT1 receptor. So, we generated a library of their conformations using the Low mode Molecular dynamics algorithm. In order to distinguish between unique conformations, 0.25 RMDS difference between structures was used without taking into account hydrogen atoms. Using this methodology, an initial pool of 28,000 conformations was generated and the three-dimensional position of their hydrogen bond donor, hydrogen bond acceptor, and hydrophobic groups was added in the database as Gaussian densities with previously defined radii. From there were selected conformations of species that shared the most common geometry of their features. The mean of the Gaussian spheres representative for their common features was the base

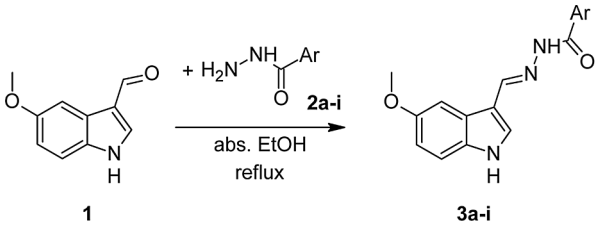

3a Ar = *p*-OH-phenyl
3b Ar = *o*-, *p*-diOH-phenyl
3c Ar = *p*-Cl-phenyl
3d Ar = *p*-F-phenyl
3e Ar = 2-furyl
3f Ar = 2-thienyl
3g Ar = *p*-OH, *m*-OMe-phenyl
3h Ar = 5-(4-methyl-1,2,3-thiadiazolyl)
3i Ar = 3-indolyl

Scheme 1. The synthetic route to the preparation of the target compounds (3a–i).

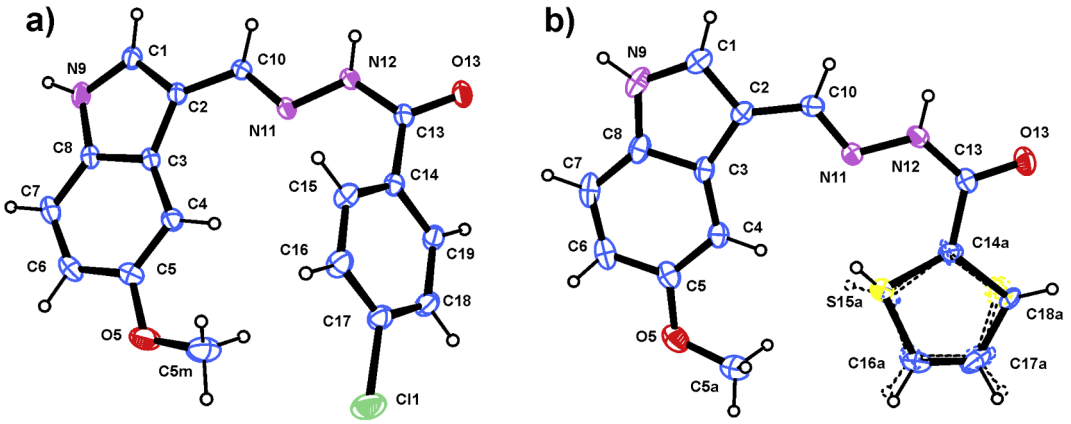

Fig. 1. ORTEP view and numbering of the molecule present in the asymmetric unit (ASU) of (a) compound **3c** and (b) compound **3f**. Atomic displacement parameters (ADP) are drawn at the 50% probability level; hydrogen atoms are shown as spheres with arbitrary radii. The thiophene ring of compound **3f** is disordered over two positions (72.3 and 27.7%) and the minor component is shown as dashed lines.

of our pharmacophore model. For the generation, the "pharmacophore elucidator" implemented in MOE2016 [MOE] software package was used.

The conformational set from which our pharmacophore model was derived is represented in Fig. 2A,B. In the used conformation's pool, a conservative motif with spatial characteristics of the amide bond is clearly seen (Fig. S4A,B), while the lipophilic parts are more nonuniform and bulky.

In our pharmacophore model depicted in Fig. S5A,B, the orange sphere, named *Aro|Hyd*, annotates *Aro* for aromatic and pseudo aromatic rings. While the *Hyd* annotations were assigned to hydrophobic groups where assigned centroids were weighted by an estimate of the likely exposed surface area of each hydrophobic atom; that is, the *Hyd* centroid placed closer to more exposed hydrophobic atoms in hydrophobic groups.

The bigger grey centroid named *Don|Acc*, represents an H-bond donor heavy atom or an H-bond acceptor heavy atom. The smaller grey sphere *Don2|Acc2* annotates projected locations of potential H-bond acceptors or projected locations of potential H-bond donors, respectively. In blue is schematically represented only *Acc2*, while the green sphere annotates *Hyd* as it is described above.

The main part of the model is planar. It consists of two areas that represent hydrophobic regions formed from ligand molecule heavy atoms connected to another one that represents set of molecule's heavy atoms capable to participate in H-bond as a donor and/or acceptor. One of that hydrophobic regions can contain a larger aromatic moiety. Centroids of these hydrophobic regions are on 4.53 and 2.21 A from the central *Don|Acc* region respectively and are connected relatively linear with an angle of 149.4° between them. The central *Don|Acc* region is also connected with other two regions that describe part of the space where potential receptor H-bond donors and/or acceptors can participate in hydrogen bonds with ligand atoms represented with central *Don|Acc* region of pharmacophore model. The angle between these three regions is 158.1°. As bigger hydrophobic region (*Aro|Hyd)* in the model can contain aromatic rings, the region where receptor parts can participate in stacking or Pi-Hbond with an aromatic ring from ligand is represented with a small orange region (*PiN*) partially immersed in bigger *Aro|Hyd* region

A library of new structures possible for synthesis was generated and was used for new conformational search task as in the case of pharmacophore elucidation. Positions of their hydrogen bond donor, hydrogen bond acceptor, and hydrophobic groups were added in the database. Species that posses conformations, which fit best in our pharmacophore model were selected for further synthesis and biological experiments.

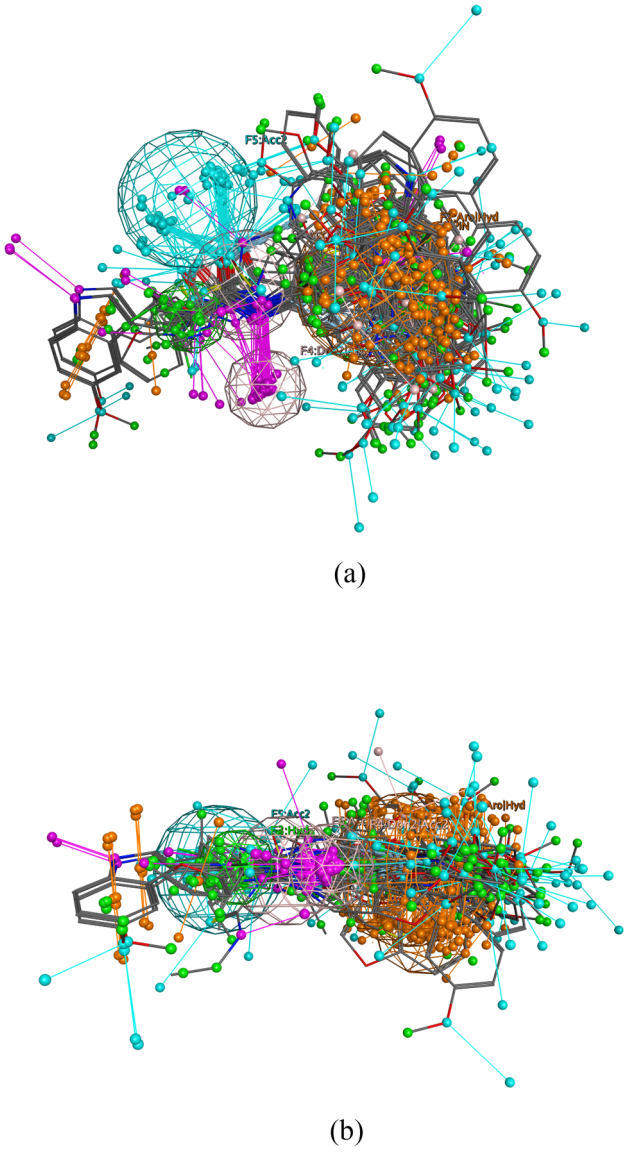

Fig. 2. (A,B) Representation of best fitted conformations of the molecules from initial set.

Table 1
Most important crystallographic and refinement parameters for **3c** and **3f**.

Compound	3c	3f
Chemical formula	$C_{17}H_{14}ClN_3O_2$	$C_{15}H_{13}N_3O_2S$
M_r	327.76	299.34
Crystal system, SG	Monoclinic, $P2_1/n$	Orthorhombic, $P2_12_12_1$
Temperature (K)	150	150
a, b, c (Å)	9.3993(5), 8.5107(3), 19.2498 (10)	6.1939(2), 14.4317(7), 15.8678(7)
α,β, γ (°)	90, 90.332(4), 90	90, 90, 90
V (Å^3)	1539.85 (13)	1418.40 (10)
Z	4	4
Radiation type	Mo $K\alpha$	Mo $K\alpha$
μ (mm^{-1})	0.26	0.24
Crystal size (mm)	0.3 × 0.25 × 0.12	0.21 × 0.18 × 0.11
Diffractometer	SuperNova, Dual, Atlas	SuperNova, Dual, Atlas
Absorption correction	Multi-scan	Multi-scan
T_{min}, T_{max}	0.578, 1.000	0.835, 1.000
No. of measured, and observed [$I > 2\sigma(I)$] reflections	8512, 2834	6212, 2290
R_{int}	0.017	0.023
$(\sin \theta/\lambda)_{max}$ (Å^{-1})	0.694	0.678
$R[F^2 > 2\sigma(F^2)]$, $wR(F^2)$, S	0.041, 0.111, 1.06	0.036, 0.088, 1.06
No. of independent reflections	3419	2756
No. of parameters	210	237
No. of restraints	0	2
H-atom treatment	constrained	constrained
$\Delta\rho_{max}$, $\Delta\rho_{min}$ (e Å^{-3})	0.27, −0.36	0.12, −0.18
Absolute structure	–	Flack × determined using 700 quotients [(I +)-(I-)]/[(I +) + (I-)]
Absolute structure parameter	–	0.05 (6) [12a]
CCDC Number	1,889,925	1,889,926

2.4. Pharmacology

2.4.1. Screening for anticonvulsant activity and neurotoxicity

The compounds were tested for anticonvulsant activity in accordance with the guidelines of the Antiepileptic Drug Development Program (ADD) of the National Institutes of Health (USA) [13]. The MES and 6 Hz test were used for preliminary screening of the novel melatonin derivatives. In parallel, the evaluation of neurotoxicity was determined via the test for minimal motor impairment (rotarod). In Phase I of evaluation, all compounds were administered intraperitoneally (i.p.), at doses of 30, 100 and 300 mg kg^{-1}, at time intervals of 0.5 h and 4 h, respectively, before seizure test. Melatonin was used as a positive control drug. The results are shown in Table 2. In the MES test, indicating an ability of active molecule to prevent the seizure spread, **3e**, carrying a 2-furyl moiety and **3f,** carrying a thienyl substituent in aroylhidrazone moiety, were the compounds effective at a dose of 100 mg kg^{-1} and 300 mg kg^{-1}, respectively, comparable to that of melatonin (Table 2). Four melatonin derivatives out of nine showed potency against the 6 Hz-induced psychomotor seizures (Table 2). The 6-Hz test is considered a model of drug-resistant epilepsy and seems to be predominantly resistant to sodium channel modulators [14].

Further, **3e** and **3f** were subjected to phase II trial to quantify its preliminary anticonvulsant activity (indicated by ED_{50}), neurotoxicity (indicated by TD_{50}) and protective index (PI) (TD_{50}/ED_{50}) in mice (Table 3). The compound **3e** and **3f** displayed ED_{50} values of 50.98 mg kg^{-1} and 108.7 mg kg^{-1}, respectively, being slightly more potent than melatonin with ED_{50} of 160.3 mg kg^{-1} in the MES test. Compounds **3c**, **3e**, **3f**, and **3i** showed activity against 6 Hz-induced psychomotor seizures suggesting that they might be efficient in partial epilepsy as well as refractory seizures in humans. The quantitative data for compounds **3c**, **3e** and **3f** revealed that **3c** carrying a *p*-chloro-substituted benzol ring, exhibited the lowest ED_{50} value of 13.98 mg kg^{-1} and PI of > 21, respectively, superior to those of other tested compounds and > 3 times higher potency compared to melatonin (ED_{50} of 49.76 mg kg^{-1} and PI of > 6.03) in the 6 Hz test in mice. Furthermore, the compound **3e** displayed ED_{50} values of 38.0 mg kg^{-1} and PI of > 7.89 and **3i** 69.35 mg kg^{-1} and > 4.33, respectively, being slightly more potent than the positive control while **3f** was less potent than melatonin with ED_{50} of 96.36 mg kg^{-1} and PI of > 3.11. In the rotarod test, novel melatonin derivatives did not display neurotoxicity at the maximum dose of 300 mg kg^{-1} compared to melatonin (Table 3).

Based on the activity of the novel melatonin derivatives, **3a** to **3i,** in comparison to positive control melatonin in the MES and 6 Hz test, the structure-activity relationship analysis suggest that the presence of a 2-furyl or a thienyl fragment in the structure of derivatives is crucial for the anticonvulsant activity in the MES test considered a test associated with seizure spread. The insertion of Cl-substituted phenyl moiety in compound **3c** increases the potency against the 6 Hz-induced psychomotor seizures > 3 times while changing with a furan moiety in the compound **3e** results in a comparable and slightly higher anti-seizure efficacy than melatonin. The presence of thienyl moiety also appeared to influence activity against 6 Hz seizures through the potency seems to be weaker than melatonin.

Careful examination of the effect of variously substituted hydrazide-hydrazone with indole scaffold showed that the presence of hydrazide-hydrazone linker with electron donating substituents in aromatic ring slightly decreases the activity of the tested compounds compared with melatonin but presence of thienyl, furyl fragments, and p-chlorophenyl moieties or 3-indole moiety respectively, in aroylhydrazone fragment led to a notable increase of anticonvulsant activity. On Fig. 3A,B,C are depicted the most promising compounds inside a representation of our pharmacophore model described above.

All of these compounds are in agreement with Lipinski rule of five [15] and fits well in our pharmacophore model with RMSD between properties of their structures and our model 0.62 A, 0.61 A and 0.53 A for **3f**, **3e** and **3c,** respectively, and that is the direction of increasing of their activity too. The original melatonin molecule fits in our model worse than these three structures with an RMSD of 1.68 A. We calculated the LogP of molecules according to the procedure implemented in MOE software ($LogP_{(Octanol/Water)}$). According to this procedure, values of 4.5, 2.6, 3.4 and 1.6 for **3c**, **3e**, **3f** and melatonin, respectively, and value for melatonin matched experimental value published in DrugBank [https://www.drugbank.ca/drugs/DB01065]. More lipophilic properties of new compounds than melatonin probably facilitate their crossing of BBB and therefore their anticonvulsant effects in the brain.

Table 2
Anticonvulsant Screening Project Phase 1 of compounds **3a-i**, intraperitoneally administered, in mice.

Compound ASP	Formula	Dose mg/kg	MES[a]		6Hz[b]		Rota-rod[c]	Classification
			0.5 h N/F	4 h N/F	0.5 h N/F	4 h N/F	0.5 h N/F	
3a	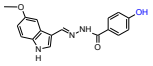	30	0/6	0/6	2/6	0/6	0/6	3
		100	0/6	0/6	2/6	0/6	0/6	
		300	1/5	0/6	3/8	0/6	0/6	
3b	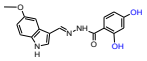	30	0/6	0/6	0/6	0/6	0/6	3
		100	0/6	0/6	1/6	0/6	0/6	
		300	0/6	0/6	2/6	0/6	0/6	
3c	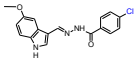	30	2/6	0/6	6/8	0/6	0/6	1
		100	0/6	0/6	7/8	0/6	0/6	
		300	1/6	0/6	7/7	0/6	0/6	
3d	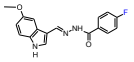	30	0/6	0/6	0/6	0/6	0/6	3
		100	1/6	0/6	2/6	0/6	0/6	
		300	0/6	0/6	2/6	0/6	0/6	
3e	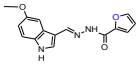	30	2/6	0/6	3/8	0/6	0/6	1
		100	5/7	0/6	7/8	0/6	0/6	
		300	2/6	0/6	7/8	0/6	0/6	
3f	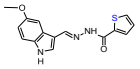	30	2/6	0/6	3/8	0/6	0/6	1
		100	0/6	0/6	4/8	0/6	0/6	
		300	6/6	0/6	3/6	0/6	0/6	
3g	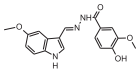	30	0/6	0/6	2/6	0/6	0/6	3
		100	1/6	0/6	0/6	0/6	0/6	
		300	0/6	0/6	1/6	0/6	0/6	
3h	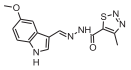	30	1/6	0/6	0/6	0/6	0/6	3
		100	1/6	0/6	1/6	0/6	0/6	
		300	0/6	0/6	2/6	0/6	0/6	
3i	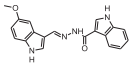	30	0/5	0/6	2/6	0/6	0/6	1
		100	1/6	0/6	4/6	0/6	0/6	
		300	1/6	0/6	1/6	0/6	0/6	
Melatonin	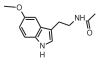	30	1/6	0/6	5/7	0/6	0/6	1
		100	2/6	0/6	9/10	0/6	0/6	
		300	6/6	0/6	4/6	0/6	0/6	
Phenytoin		30	6/6	6/6	NT	NT	0/6	1

N/F = number of animals active or toxic over the number tested; Classifications are: 1 = anticonvulsant activity at 100 mg/kg or less; 2 = anticonvulsant activity at doses > 100 mg/kg; 3 = no anticonvulsant activity at doses up to and including 300 mg/kg. NT = Not tested.

The main difference between the new compounds and melatonin molecule, according to our pharmacophore model, as it can be seen in Figs. S4 and S5, is the position of the indole ring. The benzene part of indole ring, displaced mainly outside the Aro|Hyd region in new compounds. Another difference is that in opposite to new molecules, the indole ring and ethene part in melatonin molecule was placed out of the plane of pharmacophore model.

2.4.2. Hepatotoxicity

The most active compounds were submitted for *in vitro* evaluation using rat hepatocytes, which represent a well-controlled biological model system with high drug-metabolizing capacities as a part of recommended tests from the European Centre for the Validation of Alternative Methods (ECVAM), (Blaauboer et al., 1994) [16]. Perfused rat hepatocytes are a convenient *in-vitro* system for investigating xenobiotic biotransformation and the possible mechanisms of toxic stress and its protection. For measurement of cell viability, we used Trypan blue test. Lactate dehydrogenase (LDH) is one of the most commonly used enzyme markers, as its increased release is an indicator of membrane damage [17]. Increased LDH leakage corresponds to decreased cell viability. It is known that reduced glutathione (GSH) plays an important role in cell detoxification and protection [18]. Assessment of the quantity of GSH indicates the possible toxic hepatic metabolism of xenobiotics [19]. As a biomarker of lipid peroxidation, the level of MDA

Table 3
Quantitative anticonvulsant assessment of compounds **3c, 3e, 3f** and **3i** (Phase II).

Compound	Test	TPE[a](h)	ED_{50}[b] (mg kg^{-1})	95% confidence interval	Hill slope	Standard errors of the slope	TD_{50}[c] (mg kg^{-1})	PI[d]
3c	6-Hz	0.5	13.98	(4.42–44.21)	1.30	0.33	> 300	> 21.46
3e	MES	0.5	50.98	(34.6–75.13)	1.49	0.2	> 300	> 5.88
	6-Hz	0.5	38.0	(34.07–42.40)	2.12	0.12	> 300	> 7.89
3f	MES	0.5	108.7	(62.89–187.9)	1.91	0.68	> 300	> 2.76
	6-Hz	0.5	96.36	(18.72–496.00)	2.12	0.12	> 300	> 3.11
3i	6-Hz	0.5	69.35	(50.87–94.53)	1.36	0.04	> 300	> 4.33
melatonin	MES	0.5	160.3	(97.77–262.8)	3.29	1.64	> 300	> 1.87
	6-Hz	0.5	49.76	(30.69–89.67)	1.53	0.25	> 300	> 6.03

The values represented are in the 95% confidence interval.
[a] Time to peak effect – TPE.
[b] Median effective doses (ED_{50}).
[c] Median minimal neurotoxic doses (TD_{50}).
[d] Protective index (PI) (rotarod TD_{50}/ED_{50}).

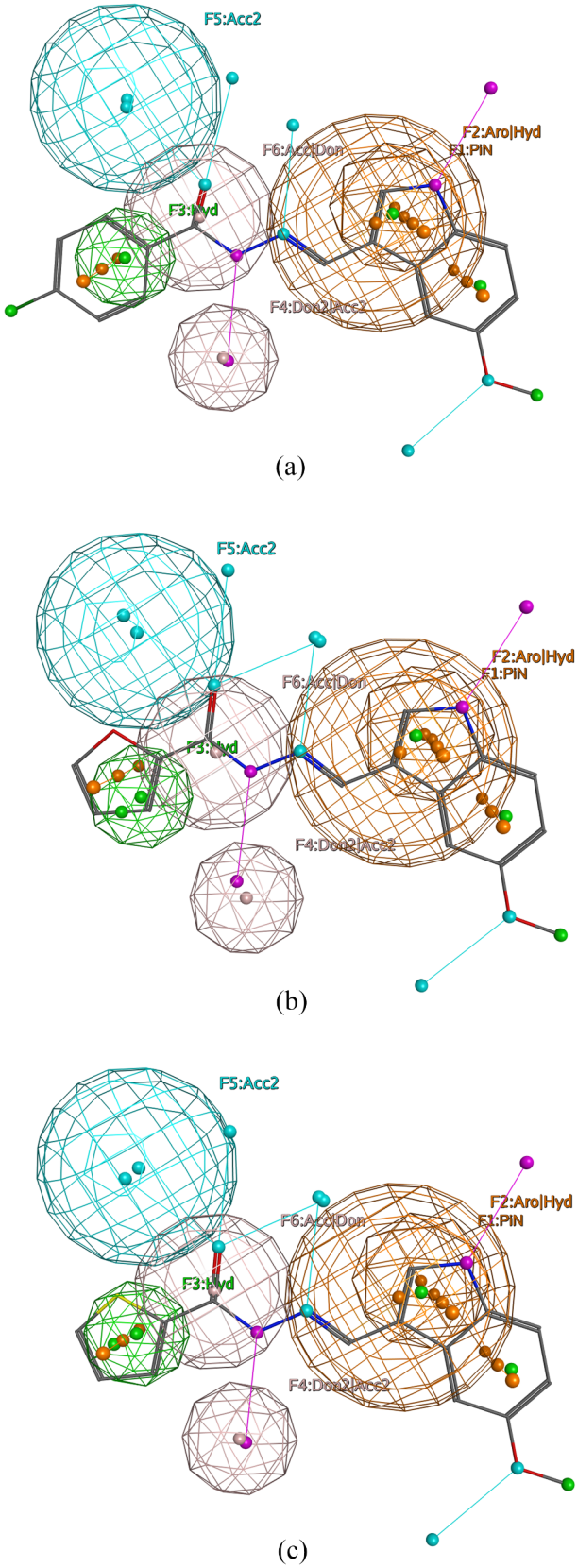

Fig. 3. The most promising compounds inside representation of our pharmacophore model. (A) **3c** compound; (B) **3e** compound; (C) **3f** compound.

was measured. In our study, the effects of melatonin derivatives, administered alone at a concentration of 100 μM, were assessed, using freshly isolated rat hepatocytes according to Gurer-Orhan et al [20].

Table 4
Effects of 100 μM **3c, 3e, 3f** and **3i** derivatives and 100 μM melatonine on parameters, characterizing functional-metabolic status of isolated rat hepatocytes.

Group	Cell viability, %	LDH, μmol/min/10^6 cell	GSH, nmol/10^6 cell	MDA, nmol/10^6 cells
Control	88 ± 3.1	0.110 ± 0.01	20 ± 1.5	0.051 ± 0.01
3c	73 ± 4.5*	0.189 ± 0.02**	11 ± 3.2*	0.089 ± 0.01**
3e	72 ± 4.2*	0.186 ± 0.05**	12 ± 2.6*	0.088 ± 0.01**
3f	81 ± 4.1	0.125 ± 0.01*	18 ± 2.6	0.060 ± 0.01*
3i	70 ± 4.1*	0.183 ± 0.01**	10 ± 3.5*	0.080 ± 0.01**
Melatonin	85 ± 3.5	0.115 ± 0.01	19 ± 2.5	0.053 ± 0.01

* $P < 0.05$.
** $P < 0.01$ vs control (non-treated hepatocytes).

The results showed that all compounds exerted weak cytotoxic effects, compared to the control (non-treated hepatocytes) (Table 4).

Melatonin did not reveal statistically significant toxic effects on the hepatocytes. The compound **3f** demonstrated the lowest cytotoxicity on the tested parameters, characterizing the functional-metabolic status of the hepatocytes. While it had comparable to melatonin non-significant effects on hepatocytes' viability and GSH level, **3f** produced a weak increase in LDH leakage with 14% and MDA production with 18%, respectively, compared to the control (non-treated hepatocytes). The compound **3c** significantly decreased cell viability with 17% and GSH level with 45%, respectively, while increased LDH leakage and MDA production with 72% and 75%, respectively, compared to the control. The compound **3i** significantly decreased cell viability with 20% and GSH level with 50%, respectively, while increased LDH leakage with 66% and MDA production with 57%, respectively, compared to the control.

The compound **3e** significantly decreased cell viability with 18% and GSH level with 40%, respectively, while increased LDH leakage with 69% and MDA production with 73%, respectively, compared to the control. On the basis of our biochemical and histopathological findings, we can conclude that compound **3f** was characterized with comparable to melatonin tested parameters.

3. Conclusions

A series of indole C-3 substituted aroylhydrazones were synthesized to explore prospective anticonvulsant agents. The pharmacophore model using for preliminary selection of potent structures for synthesis was constructed according to available drug structures targeting the MT1 receptor. The compounds **3c**, **3e**, **3f and 3i** were found to possess anticonvulsant activity in the 6 Hz test suggesting that they could be active against focal seizures. The anticonvulsant activity was strongly associated with the type and position of the substituent at the indole moiety. The compounds with a 2-furyl and 2- thienyl fragments, **3e** and **3f,** respectively, showed ED_{50} value and PI higher than melatonin in the MES test. In the 6 Hz test, the most active compound was **3c** with ED_{50} three times lower and PI higher than melatonin. None of the compounds displayed neurotoxicity in the rota-rod test. The novel melatonin derivatives exhibited low hepatoxicity. Based on the structure-activity analysis, further structural modifications of indole scaffold might lead to the discovery of more potent anticonvulsant agents in the 6 Hz test of psychomotor seizures with lower hepatotoxicity and lack of neurotoxicity.

4. Experimental procedure

4.1. Chemistry. General

The melting points were determined using a Buchi 535 apparatus and Melting point meter M5000 apparatus. The FTIR spectra were

recorded on a Nicolet IS10 FT-IR Spectrometer from Thermo Scientific (USA) using an ATR technique and FTIR spectrometer Bruker-Tenzor 27. All NMR experiments were carried out on a Bruker Avance spectrometer II + 600 MHz at 20 °C in DMSO-d_6 as a solvent, using tetramethylsilane (TMS) as an internal standard. The precise assignment of the ^{1}H and ^{13}C NMR spectra was accomplished by measurement of 2D homonuclear correlation (COSY), DEPT-135 and 2D inverse detected heteronuclear (C−H) correlations (HMQC and HMBC). Mass spectra were measured on a Q Exactive Plus mass spectrometer (ThermoFisher Scientific) equipped with aheated electrospray ionization (HESI-II) probe (ThermoScientific). All chemicals as well as compounds **1** and **2a-i** used for the synthesis were commercial products and used without further purification. The purity of the new compounds was checked by TLC on silica gel 60 GF254 Merck pre-coated aluminum sheets. The spots were visualized under UV irradiation (λ = 254 nm).

4.2. General procedure for the synthesis of compounds 3a-i

To an ethanol solution of an appropriate hydrazides **2a-i** (2.0 mmol) a stirred solution of 5-methoxyindole-3-carboxaldehyde **1** (2.0 mmol) in abs. ethanol was added. The solution was refluxed for 2–3 h. The solid product formed **3a-i** was collected by filtration and recrystallized with ethanol.

4-Hydroxy-N′-[(E)-(5-methoxy-1H-indol-3-yl)methylidene]benzohydrazide, 3a Yield: 71%; m.p. 264.5 °C; FTIR (ATR) ν_{max}: 3395O-H, 3297 N−H, 1649C = O; 1607C = N (azomethine). ^{1}H NMR (DMSO-d_6, 600 MHz): 1:0.16 mixture of conformers; signals for major synperiplanar conformer around the amide bond: δ 3.794 (s, 3H, OCH3), 6.850 (dd, J = = 2.7, 8.6 Hz, 1H, H-6), 6.859 (d, J = 8.5 Hz, 2H, H-3′ and H-5′), 7.332 (d, J = 8.8 Hz, 1H, H-7), 7.744 (d, J = 2.6 Hz, 1H, H-2), 7.812 (d, J = 8.7 Hz, 2H, H-2′ and H-6′), 7.853 (d, J = 2.3 Hz, 1H, H-4), 8.576 (s, 1H, H-8), 10.054 (brs, 1H, OH), 11.310 (brs, 1H, CONH), 11.429 (brs, 1H, NH); resolved signals for minor antiperiplanar conformer around the amide bond: 3.561 (s, 3H, OCH_3), 7.289 (d, J = 8.6 Hz, 1H, H-7), 8.228 (s, 1H, H-8), 9.974 (brs, 1H, OH), 11.109 (brs, 1H, CONH), 11.392 (brs, 1H, NH) ppm. ^{13}C NMR (DMSO-d_6, 150 MHz): δ 55.35 (OCH_3), 104.24 (C-4), 111.64 (C-3), 112.22 (C-6), 112.41 (C-7), 114.96 (C-3′ and C-5′), 124.60 (C-3a), 125.01 (C-1′), 129.43 (C-2′ and C-6′), 130.33 (C-2), 132.04 (C-7a), 144.26 (C-8), 154.38 (C-5), 160.31 (C-4′), 162.16 (C═O) ppm. HRMS (ESI) m/z: calcd: $[M+H]^+$ 310.118618. Found: $[M+H]^+$ 310.11807.

2,4-Dihydroxy-N′-[(E)-(5-methoxy-1H-indol-3-yl)methylidene] benzohydrazide, 3b Yield: 64%; m.p. 254.2 °C. FTIR (ATR) ν_{max}: 3478, 3288 OH, 3152 NH, 1640C = O, 1607C = N (azomethine), 1573C = C; ^{1}H NMR (DMSO-d_6, 600 MHz): 1:0.08 mixture of conformers; signals for major synperiplanar conformer around the amide bond: δ 3.793 (s, 3H, OCH_3), 6.292 (d, J = 2.3 Hz, 1H, H-3′), 6.351 (dd, J = 2.3, 8.7 Hz, 1H, H-5′), 6.858 (dd, J = 2.6, 8.7 Hz, 1H, H-6), 7.341 (d, J = 8.7 Hz, 1H, H-7), 7.791 (d, J = 2.8 Hz, 1H, H-2), 7.814 (d, J = 8.9 Hz, 1H, H-6′), 7.826 (d, J = 2.6 Hz, 1H, H-4), 8.583 (s, 1H, H-8), 10.166 (brs, 1H, OH), 11.434 (brs, 1H, CONH), 11.490 (brd, J = 1.7 Hz, 1H, NH), 12.782 (brs, 1H, OH); resolved signals for minor antiperiplanar conformer around the amide bond: 11.335 (brs, 1H, CONH) ppm. ^{13}C NMR (DMSO-d_6, 150 MHz): δ 55.39 (OCH_3), 102.90 (C-3′), 104.29 (C-4), 106.16 (C-1′), 107.15 (C-5′), 111.35 (C-3), 112.22 (C-6), 112.48 (C-7), 124.97 (C-3a), 129.09 (C-6′), 130.99 (C-2), 132.05 (C-7a), 145.56 (C-8), 154.49 (C-5), 162.38 (C-2′), 162.68 (C-4′), 165.16 (C═O) ppm. HRMS (ESI) m/z: calcd: $[M+H]^+$ 326.113532. Found: $[M+H]^+$ 326.11269.

4-Chloro-N′-[(E)-(5-methoxy-1H-indol-3-yl)methylidene]benzohydrazide, 3c Yield: 83%; m.p. 267–269 (267.6) °C;FTIR (ATR) ν_{max}: 3370 NH, 3297 NH, 1650(cis), 1637(trans) C═O, 1614C = N (azomethine), 1586C = C. ^{1}H NMR (DMSO-d_6, 600 MHz): 1:0.27 mixture of conformers; signals for major synperiplanar conformer around the amide bond: δ 3.794 (s, 3H, OCH_3), 6.856 (dd, J = 2.6, 8.7 Hz, 1H, H-6), 7.340 (d, J = 8.8 Hz, 1H, H-7), 7.605 (d, J = 8.5 Hz, 2H, H-3′ and H5′), 7.787 (d, J = 2.7 Hz, 1H, H-2), 7.843 (d, J = 2.5 Hz, 1H, H-4), 7.950 (d, J = 8.6 Hz, 2H, H-2′ and H-6′), 8.588 (s, 1H, H-8), 11.481 (brd, J = 1.6 Hz, 1H, NH), 11.583 (brs, 1H, CONH); resolved signals for minor antiperiplanar conformer around the amide bond: 3.459 (s, 3H, OCH_3), 7.112 (d, J = 2.5 Hz, 1H, H-4), 8.240 (s, 1H, H-8), 11.409 (brs, 1H, NH), 11.461 (brs, 1H, CONH) ppm. ^{13}C NMR (DMSO-d_6, 150 MHz): δ 55.34 (OCH_3), 104.21 (C-4), 111.42 (C-3), 112.29 (C-6), 112.48 (C-7), 124.98 (C-3a), 128.52 (C-3′ and C-5′), 129.42 (C-2′ and C-6′), 130.90 (C-2), 132.05 (C-7a), 132.82 (C-1′), 136.11 (C-4′), 145.45 (C-8), 154.47 (C-5), 161.34 (C═O). HRMS (ESI) m/z: calcd: $[M+H]^+$ 328.08430. Found: $[M+H]^+$ 328.084731.

4-Fluoro-N′-[(E)-(5-methoxy-1H-indol-3-yl)methylidene]benzohydrazide, 3d Yield: 78%; m.p. 242–243 (242.1) °C, FTIR (ATR) ν_{max}: 3153 NH, 3106 NH, 1644(cis), 1625(trans) C═O, 1611C = N (azomethine), 1572C = C; ^{1}H NMR (DMSO-d_6, 600 MHz): 1:0.19 mixture of conformers; signals for major synperiplanar conformer around the amide bond: δ 3.796 (s, 3H, OCH_3), 6.856 (dd, J = 2.6, 8.8 Hz, 1H, H-6), 7.339 (d, J = 8.9 Hz, 1H, H-7), 7.364 (t, J = 8.9 Hz, 2H, H-3′ and H-5′), 7.779 (d, J = 2.8 Hz, 1H, H-2), 7.846 (d, J = 2.5 Hz, 1H, H-4), 7.997 (dd, J = 5.5, 8.8 Hz, 2H, H-2′ and H-6′), 8.585 (s, 1H, H-8), 11.471 (brd, J = 2.0 Hz, 1H, CONH), 11.536 (brs, 1H, NH); resolved signals for minor antiperiplanar conformer around the amide bond: 3.479 (s, 3H, OCH_3), 7.715 (d, J = 2.8 Hz, 1H, H-2), 7.876 (dd, J = 5.8, 8.5 Hz, 2H, H-2′ and H-6′), 8.248 (s, 1H, H-8), 11.398 (brs, 1H, NH), 11.410 (brs, 1H, CONH) ppm. ^{13}C NMR (DMSO-d_6, 150 MHz): δ 55.34 (OCH3), 104.20 (C-4), 111.45 (C-3), 112.28 (C-6), 112.47 (C-7), 115.39 (d, J = 21.8 Hz, C-3′ and C-5′), 124.99 (C-3a), 130.12 (d, J = 8.9 Hz, C-2′ and C-6′), 130.56 (d, J = 2.9 Hz, C-1′), 130.79 (C-2), 132.05 (C-7a), 145.23 (C-8), 154.45 (C-5), 161.38 (C═O), 163.93 (d, J = 248.8 Hz, C-4′) ppm. HRMS (ESI) m/z: calcd: $[M+H]^+$ 295.118952. Found: $[M+H]^+$ 295.11844.

N′-[(E)-(5-methoxy-1H-indol-3-yl)methylidene]furan-2-carbohydrazide, 3e Yield: 81%; m.p. 222–224 °C. FTIR(ATR) ν_{max}: 3266 NH, 3211 NH, 1641(cis), 1630(trans) C═O, 1607C = N(azomethine), 1572C = C cm^{-1}; ^{1}H NMR (DMSO-d_6, 600 MHz): 1:0.23 mixture of conformers; signals for major *synperiplanar conformer* around the amide bond: δ 3.787 (s, 3H, OCH_3), 6.685 (dd, J = 1.6, 3.3 Hz, 1H, H-4′), 6.853 (dd, J = 2.5, 8.8 Hz, 3H, H-6), 7.232 (d, J = 3.3 Hz, 1H, H-5′), 7.335 (d, J = 8.7 Hz, 1H, H-7), 7.762 (d, J = 2.7 Hz, 1H, H-2), 7.819 (d, J = 2.3 Hz, 1H, H-4), 7.913 (brs, 1H, H-3′), 8.592 (s, 1H, H-8), 11.469 (brs, 1H, CONH), 11.513 (brs, 1H, NH) ppm. ^{13}CNMR (DMSO-d_6, 150 MHz): 55.75 (OCH_3), 104.67 (C-4), 111.88 (C-3), 112.41 (C-4′), 112.66 (C-6), 112.89 (C-7), 114.44 (C-5′), 125.42 (C-3a), 131.14 (C-2), 132.46 (C-7a), 145.62 (C-8), 145.77 (C-3′), 147.72 (C-1′), 154.20 (C═O), 154.87 (C-5) ppm. HRMS (ESI) m/z: calcd: $[M+H]^+$ 284.10244. Found: $[M+H]^+$ 284.102968.

N′-[(E)-(5-methoxy-1H-indol-3-yl)methylidene]thiophene-2-carbohydrazide, 3f Yield: 87%.; m.p. 201–202 (201.1) °C. FTIR (ATR) ν_{max}: 3400, 3153 N−H, 1640(cis), 1624(trans) C═O, 1611C = N (azomethine), 1581C = C. ^{1}H NMR (DMSO-d_6, 600 MHz) 1:1.06 mixture of conformers; signals for major synperiplanar conformer around the amide bond: δ 3.81 (s, 3Hs, 3H, OCH_3), 6.85 (dd, J = 2.3, 8.7 Hz, 1H, H-6), 7.22 (dd, J = 3.7, 4,9 Hz, 1H, H-4′), 7.34 (d, J = 8.7 Hz, 1H, H-7), 7.80 (d, J = 2.8 Hz, 1H, H-2), 7.85 (d, J = 2.3 Hz, 1H, H-4), 7.94 (dd, J = 1.1, 4.9 Hz, 1H, H-5′), 8.12 (dd, J = 1.1, 3.7 Hz, 1H, H-3′), 8.31 (s, 1H, H-8), 11.44 (brs, 1H, CONH), 11.56 (brs, 1H, NH); signals for minor antiperiplanar conformer around the amide bond: δ 3.79 (s, 3H, OCH_3), 6.86 (dd, J = 2.3, 8.7 Hz, 1H, H-6), 7.21(dd, J = 3.7, 4,9 Hz, 1H, H-4′), 7.36 (d, J = 8.7 Hz, 1H, H-7) 7.79 (d, J = 2.8 Hz, 1H, H-2), 7.82 (d, J = 2.3 Hz, 1H, H-4), 7.83 (dd, J = 1.1, 4.9 Hz, 1H, H-5′), 7.89 (dd, J = 1.1, 3.7 Hz, 1H, H-3′), 8.58 (s, 1H, H-8), 11.48 (brs, 1H, NH), 11.56 (brs, 1H, CONH) ppm. ^{13}C NMR (DMSO-d_6, 150 MHz) signals for major synperiplanar conformer δ 55.41 (OCH_3), 102.48 (C-4), 111.09 (C-3), 111.42 (C-3), 112.83 (C-7), 113.11 (C-6), 124.11 (C-3a), 126.77 (C-4′), 131.79 (C-2), 131.93 (C-7a), 133.39 (C-5′), 133.69 (C-3′), 134.33 (C-2′), 142.31 (C-8), 154.45 (C-5), 160.59 (C═O); signals for minor

antiperiplanar conformer 55.30 (OCH_3), 104.10 (C-4), 112.30 (C-6), 112.47 (C-7), 124.95 (C-3a), 128.03 (C-4′), 128.11 (C-3′), 130.77 (C-2), 131.10 (C-5′), 132.02 (C-7a), 139.17 (C-2′), 145.00 (C-8), 154.60 (C-5), 157.15 (C═O) ppm. HRMS (ESI) *m/z*: calcd: $[M+H]^+$ 300.080123. Found: $[M+H]^+$ 300.07952.

4-Hydroxy-3-methoxy-N′-[(E)-(5-methoxy-1H-indol-3-yl)methylidene]benzohydrazide, 3 g Yield: 52%; m.p. 182–184/192 °C; FTIR (ATR) ν_{max}: 3334, 3154 N−H, 1644(cis), 1628(trans) C═O,1613C = N (azomethine). ^{1}H NMR (600 MHz, DMSO-d_6) δ 11.433 (d, J = 2.7 Hz, 1H, NH), 11.298 (brs, 1H, CONH), 9.647 (brs, 1H, OH), 8.588 (s, 1H, H-8), 7.857 (d, J = 2.6 Hz, 1H, H-4), 7.748 (d, J = 2.7 Hz, 1H, H-2), 7.504 (d, J = 1.9 Hz, 1H, H-2′), 7.448 (dd, J = 1.9, 8.2 Hz, 1H, H-6′), 7.334 (d, J = 8.8 Hz, 1H, H-7), 6.868 (d, J = 8.2 Hz, 1H, H-5′), 6.848 (dd, J = 2.6, 8.8 Hz, 1H, H-6), 3.855 (s, 3H, OCH_3-C-5), 3.795 (s, 3H, OCH_3-C-3′) ppm. ^{13}C NMR (151 MHz, DMSO-d_6) δ 162.07 (C═O), 154.37 (C-5), 149.68 (C-4′), 147.25 (C-3′), 144.33 (C-8), 132.00 (C-7a), 130.28 (C-2), 124.99 (C-3a), 124.85 (C-1′), 120.93 (C-6′), 114.90 (C-5′), 112.41 (C-7), 112.28 (C-6), 111.61 (C-3), 111.50 (C-2′), 104.11 (C-4), 55.69 (OCH_3-C-5), 55.29 (OCH_3-C-3′) ppm. HRMS (ESI) *m/z*: calcd: $[M+H]^+$ 340.129182. Found: $[M+H]^+$ 340.12878.

N′-[(E)-(5-methoxy-1H-indol-3-yl)methylidene]-4-methyl-1,2,3-thiadiazole-5-carbohydrazide, 3 h. Yield: 92%; m.p. 260.2 °C. FTIR (ATR) ν_{max}: 3234 NH, 3137 NH, 1658, 1627C = O, 1603C = N 1585C = C cm^{-1}; ^{1}H NMR (DMSO-d_6, 600 MHz): 1:0.07 mixture of-conformers; signals for major *synperiplanar conformer* around the amide bond: δ 2.970 (s, 3H, CH_3), 3.828 (s, 3H, OCH_3), 6.876 (dd, J = 2.5, 8.8 Hz, 1H, H-6), 7.381 (d, J = 8.8 Hz, 1H, H-7), 7.697 (d, J = 2.3 Hz, 1H, H-4), 7.907 (d, J = 2.9 Hz, 1H, H-2), 8.382 (s, 1H, H-8), 11.706 (brs, 1H, NH), 12.022 (brs, 1H, CONH) ppm. ^{13}C NMR (DMSO-d_6, 150 MHz): 15.26 (CH_3), 55.83 (OCH_3), 102.67 (C-4), 110.92 (C-3), 113.53 (C-6 and C-7), 124.44 (C-3a), 132.44 (C-7a), 133.30 (C-2), 136.91 (C-1′), 144.16 (C-8), 155.20 (C-5), 159.42 (C═O), 163.05 (C-5′) ppm. HRMS (ESI) *m/z*: calcd: $[M+H]^+$ 316.08565. Found: $[M+H]^+$ 316.086271.

N′-[(E)-(5-methoxy-1H-indol-3-yl)methylidene]-1H-indole-3-carbohydrazide, 3i. Yield: 64%; m.p. 235–236 °C; FTIR (ATR) ν_{max}: 3320 NH, 3138 NH, 1627C = O, 1604C = N 1578C = C cm^{-1}; ^{1}H NMR (600 MHz, DMSO-d_6, 373 K) δ 3.798 (s, 3H, CH_3O), 6.859 (dd, J = 2.5, 8.7 Hz, 1H, H-6), 7.136 (ddd, J = 1.1, 6.9, 7.9 Hz, 1H, H-5′), 7.182 (ddd, J = 1.1, 6.9, 8.0 Hz, 1H, H-6′), 7.346 (dd, J = 0.5, 8.7 Hz, 1H, H-7), 7.472 (ddd, J = 0.9, 1.1, 8.0 Hz, 1H, H-7′), 7.636 (d, J = 2.75 Hz, 1H, H-2), 7.777 (d, J = 2.5 Hz, 1H, H-4), 8.234–8.252 (m, 2H, H-2′ and H-4′), 8.511 (s, 1H, H-8), 10.565 (brs, 1H, NHCO), 11.081 (brs, 1H, NH-1), 11.386 (brs, 1H, NH-1′). ^{13}C NMR (151 MHz, DMSO-d_6) δ 55.22 (CH_3O), 103.73 (C-4), 108.97 (C-3′), 111.13 (C-7′), 111.43 (C-3), 111.76 (C-7), 111.91 (C-6), 119.80 (C-5′), 120.81 (C-4′), 121.36 (C-6′), 126.43 (C-3a), 126.63 (C-3a'), 128.43 (C-2′), 128.79 (C-2), 131.77 (C-7a), 135.61 (C-7a'), 141.53 (C-8), 154.16 (C-5), 161.83 (C═O). HRMS (ESI) *m/z*: 333.134602. HRMS (ESI) *m/z*: calcd: $[M+H]^+$ 333.134602. Found: $[M+H]^+$ 333.13460.

4.3. Single crystal X-ray diffraction

The compounds **3c** and **3f** ware obtained as single crystals by slow evaporation from an ethanol solution of the pure compound at room temperature. Suitable single crystals of the compounds **3c** and **3f** were mounted on glass capillaries. The intensity and diffraction data were collected on Agilent SupernovaDual diffractometer equipped with an Atlas CCD detector using micro-focus Mo $K\alpha$/radiation (λ = 0.7107 Å, respectively). The structures were solved by direct methods and refined by the full-matrix least-squares method on F^2 with ShelxS and ShelxL programs [21]. All non-hydrogen atoms, including solvent molecules, were located successfully from Fourier map and were refined anisotropically. The hydrogens of N atoms were located from Fourier map and refined freely while the remaining hydrogens were placed at calculated positions using a riding scheme (*Ueq* = 1.2 for C-$H_{aromatic}$ and C−H = 0.94 Å and *Ueq* = 1.5 for C-H_{methyl} and of C−H = 0.97 Å). The ORTEP[22] views of the molecules present in the asymmetric unit and the most important crystallographic parameters from the data collection and refinement are shown in Fig. 1 and Table 1 respectively. Selected bonds lengths, angles and torsion angles are given in Table S1. The figures concerning crystal structure description and comparison were prepared using Mercury software (version 3.9) [23].

CCDC 1,889,925 and 1,889,926 contain the supplementary crystallographic data for compounds **3c** and **3f**. These data can be obtained free of charge from The Cambridge Crystallographic Data Centre *via* www.ccdc.cam.ac.uk/structures.

4.4. Pharmacophore modeling

In our study we used MOE 2016 software package for both pharmacophore elucidation and for testing of new drug candidates with the model. All described algorithms were used as they were implemented in the MOE software.

4.5. Pharmacology

4.5.1. Animals and treatment

Male ICR mice (25–30 g) and Wistar rats (250–300 g) were kept under standard laboratory conditions, 22 ± 1 °C, in groups of six per cage and allowed free access to food and water. All procedures were performed in agreement with the European Communities Council Directive 2010/63/EU. Control group (treated with vehicle) and experimental groups (treated with the novel compounds) were injected i.p. at different doses and were dissolved in 10% DMSO, at a volume of 10 ml kg^{-1}. Procedures used for exploration of anticonvulsant activity and neurotoxicity were described elsewhere[24]. The anticonvulsant activity of the tested compounds was evaluated by maximal electroshock test (MES) and 6 Hz test, respectively, in mice at 0.5 h after their injection. Melatonin was used as a positive control. The rotarod test was applied to evaluate the neurotoxicity of the compounds. The experimental design was approved by the Institutional Ethics Committee at the Institute of Neurobiology.

4.5.2. MES test

Before using electric stimulus of 50 mA, 60 Hz delivered for 0.2 s (Constant Current Shock Generator) through corneal electrodes, a drop of a local anesthetic was applied to the eyes of tested animal. The criterion for anticonvulsant activity of the compound was a suppression of the tonic component with an abolition of the hind limb extensor component of seizure in half or more of the animals.

4.5.3. 6-Hz psychomotor seizure test

For the 6-Hz seizure test, the electric stimulus of 32 mA, 6 Hz delivered for 3 s was delivered through corneal electrodes to assess the efficacy of the compounds against psychomotor seizures in 97% of animals. The seizure in the controls is characterized by a minimal clonic phase followed by stereotyped, automatistic behaviors, including twitching of the vibrissae, and Straub-tail. If the animal resumed its normal exploratory behavior within 10 s after stimulation this was considered as a protection.

4.5.4. Neurotoxicity screening in mice

The minimal motor impairment was measured by a standardized rota-rod test. The mouse was placed on rotating 3.2 cm in diameter rod at a speed 10 rpm. A criterion for neurotoxicity was accepted by the inability of the animal to stay on the rod for at least one minute in each of the three trials. The dose at which 50% of the animals were unable to balance themselves and fell off the rotating rod was determined as toxic.

4.5.5. Cytoxicity screening. Chemicals

The chemicals used in the experiments were: pentobarbital sodium (Sanofi, France), HEPES (Sigma Aldrich, Germany), NaCl (Merck, Germany), KCl (Merck), D-glucose (Merck), $NaHCO_3$ (Merck), KH_2PO_4 (Scharlau Chemie SA, Spain), $CaCl_2{\cdot}2H_2O$ (Merck), $MgSO_4{\cdot}7H_2O$ (Fluka AG, Germany), collagenase from *Clostridium histolyticum* type IV (Sigma Aldrich), albumin, bovine serum fraction V, minimum 98% (Sigma Aldrich), EGTA (Sigma Aldrich), 2-thiobarbituric acid (4,6-dihydroxypyrimidine-2-thiol; TBA) (Sigma Aldrich), trichloroacetic acid (TCA) (Valerus, Bulgaria), 2,2′-dinitro-5,5′-dithiodibenzoic acid (DTNB) (Merck), lactate dehydrogenase (LDH) kit (Randox, UK), *tert*-butyl hydroperoxide (Sigma Aldrich), carbon tetrachloride (Merck).

4.5.6. Isolation and incubation of hepatocytes

Rats were anesthetized with sodium pentobarbital (0.2 ml/100 g). An optimized *in situ* liver perfusion using less reagents and shorter time of cell isolation was performed. The method provided in higher amount of live and metabolically active hepatocytes [25]. After portal catheterization, the liver was perfused with HEPES buffer (pH = 7.85) + 0.6 mM EDTA (pH = 7.85), followed by clean HEPES buffer (pH = 7.85) and finally HEPES buffer containing collagenase type IV (50 mg/200 ml) and 7 mM $CaCl_2$ (pH = 7.85). The liver was excised, minced into small pieces, and hepatocytes were dispersed in Krebs-Ringer-bicarbonate (KRB) buffer (pH = 7.35) + 1% bovine serum albumin. Cells were counted under the microscope and the viability was assessed by Trypan blue exclusion (0.05%) (Fau et al., 1992). Initial viability averaged 89%. Cells were diluted with KRB to make a suspension of about $3x10^6$ hepatocytes/ml. Incubations were carried out in flasks containing 3 ml of the cell suspension (i.e. 9×10^6 hepatocytes) and were performed in a 5% CO_2 + 95% O_2 atmosphere.

4.5.7. Biochemical assays. Lactate dehydrogenase (LDH) release

After incubation, the hepatocytes were centrifuged for 4 min at 500 rpm and the supernatant was used for measuring LDH release spectrophotometrically by LDH kit [26].

4.5.7.1. Reduced glutathione (GSH) depletion. At the end of the incubation, isolated rat hepatocytes were centrifuged (at 4 °C) and the pellet was used for evaluation the level of intracellular GSH. It was assessed by measuring non-protein sulfhydryls after precipitation of proteins with trichloroacetic acid (TCA), followed by measurement of thiols in the supernatant with DTNB. The absorbance was measured at 412 nm [26].

4.5.7.2. Malondialdehyde (MDA) assay. After incubation, 1 ml from hepatocyte suspension was taken and added to 0.67 ml of 20% (w/v) TCA. After centrifugation, 1 ml of the supernatant was added to 0.33 ml of 0.67% (w/v) 2-thiobarbituric acid (TBA) and heated at 100 °C for 30 min. The absorbance was measured at 535 nm, and the amount of TBA-reactants was calculated using a molar extinction coefficient of MDA $1.56 \times 10^5\ M^{-1}cm^{-1}$ (13).

4.6. Statistical analysis

The ED_{50} (the dose effective in 50% of tested animals) and TD_{50} (the dose toxic in 50% of tested animals) were calculated by means of probit analysis with 95% confidence interval in the quantitative analysis of *in vivo* data. *In-vitro* data were expressed as mean ± SEM for 6 experiments. The significance of the data was assessed by using the non-parametric Mann–Whitney *U* test (MEDCALC). A level of $p < 0.05$ and $p < 0.01$ was considered significant.

Acknowledgements

This project was financially supported by the National Science Fund of Bulgaria, Grant DN 13/16 21.12.2017. The authors are thankful to Nikolay Vassilev and Nadezhda Yanakieva for excellent technical assistance.

Declaration of Competing Interest

The authors declare that they have no competing interests.

Appendix A. Supplementary material

Supplementary data to this article can be found online at https://doi.org/10.1016/j.bioorg.2019.103028.

References

[1] R. Jockers, P. Delagrange, M.L. Dubocovich, R.P. Markus, N. Renault, G. Tosini, E. Cecon, D.P. Zlotos, Update on melatonin receptors: IUPHAR Review 20, Brit. J. Pharmacol. 173 (18) (2016) 2702–2725.
[2] G. O'Neal-Moffitt, V. Delic, P. Bradshaw, J. Olcese, Prophylactic melatonin significantly reduces Alzheimer's neuropathology and associated cognitive deficits independent of antioxidant pathways in AβPP swe/PS1 mice, Mol. Neurodegener. 10 (1) (2015) 27.
[3] H.-A. Yamamoto, P.V. Mohanan, Effect of α-ketoglutarate and oxaloacetate on brain mitochondrial DNA damage and seizures induced by kainic acid in mice, Toxicol. Lett. 143 (2) (2003) 115–122.
[4] P.A. Forcelli, J. Kim, A. Kondratyev, K. Gale, Pattern of antiepileptic drug–induced cell death in limbic regions of the neonatal rat brain, Epilepsia 52 (12) (2011) e207–e211.
[5] K. Fenoglio-Simeone, A. Mazarati, S. Sefidvash-Hockley, D. Shin, J. Wilke, H. Milligan, R. Sankar, J.M. Rho, R. Maganti, Anticonvulsant effects of the selective melatonin receptor agonist ramelteon, Epilepsy Behav. 16 (1) (2009) 52–57.
[6] F. Brigo, A. Del Felice, Melatonin as add-on treatment for epilepsy, Cochrane Database Syst. Rev. (2012) 6.
[7] J. Uberos, M. Augustin-Morales, A. Molina Carballo, J. Florido, E. Narbona, A. Muñoz-Hoyos, Normalization of the sleep–wake pattern and melatonin and 6-sulphatoxy-melatonin levels after a therapeutic trial with melatonin in children with severe epilepsy, J. Pineal Res. 50 (2) (2011) 192–196.
[8] C. Legros, S. Devavry, S. Caignard, C. Tessier, P. Delagrange, C. Ouvry, J.A. Boutin, O. Nosjean, Melatonin MT1 and MT2 receptors display different molecular pharmacologies only in the G-protein coupled state, Brit. J. Pharmacol. 171 (1) (2014) 186–201.
[9] A. Oishi, E. Cecon, R. Jockers, Melatonin receptor signaling: impact of receptor oligomerization on receptor function, Int. Rev. Cell Mol. Biol., Elsevier 338 (2018) 59–77.
[10] R.O. Dror, H.F. Green, C. Valant, D.W. Borhani, J.R. Valcourt, A.C. Pan, D.H. Arlow, M. Canals, J.R. Lane, R. Rahmani, Structural basis for modulation of a G-protein-coupled receptor by allosteric drugs, Nature 503 (7475) (2013) 295.
[11] P.F. Oliveira, B. Guidetti, A. Chamayou, C. André-Barrès, J. Madacki, J. Korduláková, G. Mori, B.S. Orena, L.R. Chiarelli, M.R. Pasca, Mechanochemical synthesis and biological evaluation of novel isoniazid derivatives with potent antitubercular activity, Molecules 22 (9) (2017) 1457.
[12] S. Parsons, H.D. Flack, T. Wagner, Use of intensity quotients and differences in absolute structure refinement, Acta Crystallogr. Sect. B 69 (2013) (3), 249–259; (b) G. Sheldrick, Crystal structure refinement with SHELXL, Acta Crystallogr. Sect. C 71 (2015) (1), 3–8; (c) D.P. Singh, B.K. Allam, R. Singh, K.N. Singh, V.P. Singh, A binuclear Cu(i) complex as a novel catalyst towards the direct synthesis of N-2-aryl-substituted-1,2,3-triazoles from chalcones, RSC Adv. 6 (2016) (19), 15518–15524.
[13] R. Krall, J. Penry, B. White, H. Kupferberg, E. Swinyard, Antiepileptic drug development: II. Anticonvulsant drug screening, Epilepsia 19 (4) (1978) 409–428.
[14] H. Potschka, Animal models of drug-resistant epilepsy, Epileptic Disorders 14 (3) (2012) 226–234.
[15] C.A. Lipinski, F. Lombardo, B.W. Dominy, P.J. Feeney, Experimental and computational approaches to estimate solubility and permeability in drug discovery and development settings, Adv. Drug Deliv. Rev. 23 (1–3) (1997) 3–25.
[16] B. Blaauboer, A. Boobis, J. Castell, S. Coecke, M. Groothuis, A. Guillouzo, T. Hall, G. Hawksworth, G. Lorenzon, H. Miltenburger, Practical applicability of hepatocyte cultures in routine testing: the report and recommendations of ECVAM Workshop 1. Alternatives to laboratory animals: ATLA, 1994.
[17] C. Guguen-Guillouzo, A. Guillouzo, Human hepatocyte cul-tures. In vitro biological systems. Methods Toxicol., 1 (1986) 271–278.
[18] T.M. Bray, C.G. Taylor, Tissue glutathione, nutrition, and oxidative stress, Canad. J. Physiol. Pharmacol. 71 (9) (1993) 746–751.
[19] R. Glöckner, D. Müller, Ethoxycoumarin O-deethylation (ECOD) activity in rat liver slices exposed to beta-naphthoflavone (BNF) in vitro, Exp. Toxicol. Pathol. 47 (4) (1995) 319–324.
[20] H. Gurer-Orhan, C. Karaaslan, S. Ozcan, O. Firuzi, M. Tavakkoli, L. Saso, S. Suzen, Novel indole-based melatonin analogues: Evaluation of antioxidant activity and protective effect against amyloid β-induced damage, Bioorg. Med. Chem. 24 (8) (2016) 1658–1664.
[21] Z. Che, S. Zhang, Y. Shao, L. Fan, H. Xu, X. Yu, X. Zhi, X. Yao, R. Zhang, Synthesis and Quantitative Structure-Activity Relationship (QSAR) Study of Novel N-Arylsulfonyl-3-acylindole arylcarbonyl hydrazone derivatives as nematicidal

agents, J. Agric. Food Chem. 61 (24) (2013) 5696–5705.
[22] L. Farrugia, WinGX and ORTEP for Windows: an update, J. Appl. Crystallogr. 45 (4) (2012) 849–854.
[23] C.F. Macrae, I.J. Bruno, J.A. Chisholm, P.R. Edgington, P. McCabe, E. Pidcock, L. Rodriguez-Monge, R. Taylor, J. van de Streek, P.A. Wood, C.S.D. Mercury, 2.0 - new features for the visualization and investigation of crystal structures, J. Appl. Crystallogr. 41 (2) (2008) 466–470.
[24] V.T. Angelova, Y. Voynikov, P. Andreeva-Gateva, S. Surcheva, N. Vassilev, T. Pencheva, J. Tchekalarova, In vitro and in silico evaluation of chromene based aroyl hydrazones as anticonvulsant agents, Med. Chem. Res. 26 (9) (2017) 1884–1896.
[25] M. Mitcheva, M. Kondeva, V. Vitcheva, P. Nedialkov, G. Kitanov, Effect of benzophenones from Hypericum annulatum on carbon tetrachloride-induced toxicity in freshly isolated rat hepatocytes, Redox Rep.: Commun. Free Radic. Res. 11 (1) (2006) 3–8.
[26] D. Fau, A. Berson, D. Eugene, B. Fromenty, C. Fisch, D. Pessayre, Mechanism for the hepatotoxicity of the antiandrogen, nilutamide. Evidence suggesting that redox cycling of this nitroaromatic drug leads to oxidative stress in isolated hepatocytes, J. Pharmacol. Exp. Therapeut. 263 (1) (1992) 69–77.